ISSN:1983 7402

ITA, 25 a 28 de setembro de 2012

Effect of Fiber Optic Chromatic Dispersion on the Performance of Analog Optical Link with Dual-Drive Mach-Zehnder Modulator

Antonio Alves Ferreira Júnior[1], Olympio Lucchini Coutinho[2], Carla de Sousa Martins[3], William dos Santos Fegadolli[2], José Antônio Justino Ribeiro[1], and José Edimar Barbosa Oliveira[2]

[1]Instituto Nacional de Telecomunicações – INATEL, Avenida João de Camargo 510, Santa Rita do Sapucaí, 37540-000, MG, Brasil

[2]Instituto Tecnológico de Aeronáutica – ITA, Praça Marechal Eduardo Gomes, 50, São José dos Campos, 12228-900, SP, Brasil

[3]Instituto de Pesquisas da Marinha – IPqM, Rua Ipiru, 02, Rio de Janeiro, 21931-095, RJ, Brasil

***Abstract* — This paper addresses the subject of fiber optic chromatic dispersion effect on the performance of analog optical link with dual-drive electrooptic Mach-Zehnder modulator. To this aim a direct detection link model which emphasizes both the modulator electronic drive and the dispersion characteristic of a linear optical fiber is discussed. Furthermore, a mathematical approach which yields a rather insightful analysis of the link performance for either ODSB or OSSB optical modulation formats is fully discussed. It is worthwhile to point out that such modeling has the special feature of relying on a uniform nomenclature which enables one to quickly retrieve a wide range of known results regarding to optical fiber link performance, which are already available on a rather ample literature. The model usefulness is illustrated by predicting the dependence of the performance of a direct detection fiber optic link with respect to the RF frequency and link length. Results of numerical simulations for a link which comprises state of the art optoelectronic components and has potential for practical application on electronic warfare field are given.**

***Key words* — Dual-Drive Mach-Zehnder modulator, fiber optic link, and chromatic dispersion.**

I. Introduction

Nowadays, due to the increasing evidence that radio over fiber technology will be playing a major role in the global interconnectivity, a lot of efforts have been directed toward researches and development on the field of fiber optic link. A great deal of such efforts continues to be driven by important commercial and military demands, which aim at previously unachievable performance on the subjects of RF/microwave signal processing, radio-over-fiber, and antenna-remoting, [1]-[5]. This publication is concerned with the effect of fiber optic chromatic dispersion on the performance of links which operate based on external intensity modulation and direct detection techniques, i.e., the so called IM/DD optical links configuration. A typical schematic representation of the IM/DD link is shown in Fig. 1. At the input end of such links an optical laser diode generates a carrier at a desired optical wavelength, and a dual-drive electrooptic Mach-Zender modulator (DD-MZM) imposes an analog radiofrequency (RF) signal on the optical carrier, whereas at the output end of the link a photodetector (PD) is employed to recover the analog RF signal from its optical carrier. It is worthwhile to point out that the DD-MZM plays an important role in the link because it enables the wideband implementation of either optical single sideband (OSSB) or optical double sideband (ODSB) modulation formats.

A. A. Ferreira Júnior, antonioa@inatel.br; O. L. Coutinho, olympio@ita.br; C. S. Martins, carla@ipqm.mar.mil.br; W. S. Fegadolli, fegadoli@ita.br; J. A. J. Ribeiro, justino@inatel.br; J. E. B. Oliveira, edimar@ita.br.

Assuming a balanced 50/50 splitting ratio of the DD-MZM's Y-junctions, a rigorous analysis of the chromatic dispersion effect on the performance of the analog link illustrated in Fig. 1 is given by [6] but the expressions there are in the form of infinite series. Such drawback is overcome in [7] where an analytical model in which the modulation indexes of the two DD-MZM drives can be unbalanced, yields a simple closed-form expressions for the power at the output of the detector. However, fabrication tolerances make a balanced 50/50 DD-MZM's particularly difficult to achieve, hence practical modulators have a finite extinction rate. Therefore, a general model which permits the study of all these cases will be very helpful for system design.

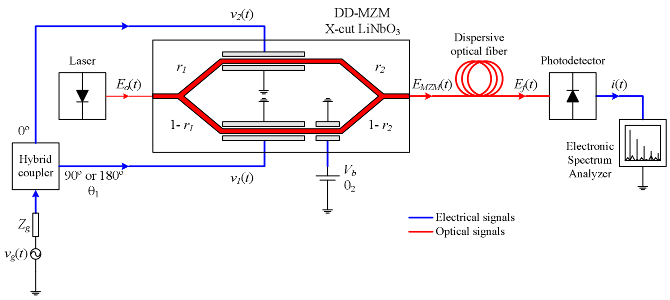

Fig. 1. Overall architecture of the IM/DD analog fiber optic link consisting of a DD-MZM, spool of single mode fiber optic, and a photodetector.

This publication consists of four sections beyond this introduction. The statement of the problem, which comprises an overview of the optical link components, is given in Section II. An analytical frequency-domain model for a single RF ton analog fiber optic link which takes into account the Graf's addition theorem for Bessel functions is fully discussed in Section III. Such formulation beyond allowing one to retrieve results presented in various publications it enables an insightful understanding of the generation of both the ODSB and the OSSB modulation formats. Numerical simulated results are presented and discussed in Section IV. A few conclusions are presented in Section V.

II. Statement of the Problem

As mentioned before at the input of the fiber optic link a continuous wave from a distributed feedback single mode laser diode (DFB-LD), generates an optical carrier at a desired wavelength/frequency with a complex optical field represented by [4],[5]

$$E_o(t) = \sqrt{2\xi P_o(t)}\, e^{j[\omega_o t + \phi_o(t)]} \tag{1}$$

where ω_o is the mean optical frequency, $\phi_o(t)$ is the phase, $P_o(t)$ is the optical power, and $\xi\left[\Omega/\mathrm{m}^2\right]$ is a constant which depends on both the laser beam effective cross section and the optical wave impedance. It is worthwhile to point out that the electric field should obey the following Fourier transform pair

$$E_o(\omega)=\int_{-\infty}^{+\infty}E_o(t)e^{-j\omega t}dt \tag{2.a}$$

$$E_o(t)=\frac{1}{2\pi}\int_{-\infty}^{+\infty}E_o(\omega)e^{j\omega t}d\omega \tag{2.b}$$

This publication relies on the often used approach in the analysis of IM/DD optical links, according to which the laser average power and its phase are time invariant [6],[7]. Therefore, under such assumptions (1) can be rewritten as

$$E_o(t)=\sqrt{2\xi P_o}\,e^{j\omega_o t} \tag{3}$$

Returning to Fig. 1, one notices that the optical power delivered by the laser diode reaches the input Y-junction of the integrated optic DD-MZM with a X-cut $LiNbO_3$ substrate, and then is divided into two parcels according to a splitting ratio [8], determined by the Y-junction power transmission coefficient r_1. The chosen substrate crystal cut orientation has the advantage of minimizes the fraction of chirping effect caused by the substrate properties [9]-[11]. As a consequence of the electrooptic effect a RF signal can be used to control the phase of the optical field associated with each optical power parcels as they propagates through the distinct arms of the DD-MZM. The RF signal, henceforth named modulation signal, must generates an electric field having both a temporal and a spatial patterns adequately distribute in order to reach some key requirements performance, such as low RF power consumption and wide RF bandwidth [12]-[14]. A great deal of such control may be achieved through the drive electronics, by properly choosing the phase shift (θ_1) and the bias (θ_2) of the electrical signal applied to the modulator electrodes, as indicated in Fig. 1 [6],[7],[15]. According to this figure, the instantaneous values of the modulating signals applied to the lower and upper electrodes of MZM, are given, respectively, by

$$v_1(t)=V_1\cos(\omega_{RF}t+\theta_1) \tag{4}$$

$$v_2(t)=V_2\cos(\omega_{RF}t) \tag{5}$$

where V_1 and V_2 are the signals amplitudes in the lower and upper arms, ω_{RF} is the angular frequency of RF signal, and θ_1 is the phase difference between the signals. The optical phase variations introduced in the arms of the modulator through linear electrooptic effect are given by

$$\phi_1(t)=\frac{\pi v_1(t)}{V_\pi}=m_1\cos(\omega_{RF}t+\theta_1) \tag{6}$$

$$\phi_2(t)=\frac{\pi v_2(t)}{V_\pi}=m_2\cos(\omega_{RF}t) \tag{7}$$

$$\phi_b(t)=\frac{\pi V_b}{V_\pi}=\theta_2 \tag{8}$$

where V_π is the half-wave switching voltage of the MZM, θ_2 is the phase variation due the bias in the lower arm, and m_1 e m_2 are the modulation indexes due the modulating signals in the lower and upper arms, respectively

$$m_1=\frac{\pi V_1}{V_\pi} \tag{9}$$

$$m_2=\frac{\pi V_2}{V_\pi} \tag{10}$$

Based on the schematic representation shown in Fig. 1 and taking into account the splitting ratio of the output Y-junction r_2, it can be shown that the optical electrical field at the output of the DD-MZM, has a complex form given by

$$\begin{aligned}E_{MZM}(t)= \; & E_o e^{j\omega_o t}\Big\{\sqrt{r_1 r_2}\,e^{j\left[m_1\cos(\omega_{RF}t+\theta_1)+\theta_2\right]}+\\ & +\sqrt{(1-r_1)(1-r_2)}\,e^{jm_2\cos(\omega_{RF}t)}\Big\}\end{aligned} \tag{11}$$

where

$$E_o=\sqrt{2\xi P_o} \tag{12}$$

It will be shown later in this publication that the MZM's output field in frequency domain consists of a carrier component at ω_o and an infinite number of sidebands. It should be pointed out that (11) applies to DD-MZM having both arbitrary splitting ratios and modulation signals. Such general situation often occurs in the real world, either at the modulator's fabrication stage or in field applications. Based on (11), the authors have been investigating the chirp modeling of DD-MZM as a function of both the splitting rations and modulation indexes. The obtained results will be published elsewhere. Furthermore, (11) enables one quickly retrieve the results for DD-MZM having infinite extinction when the splitting rations obey the constraints $r_1=r_2=0.5$.

At this stage of this publication, it is convenient returning to Fig. 1, to observe that the optical signal at the output of the modulator, with electric field given by (11), feeds a spool of standard single-mode optical fiber (SSMF), with length L. In order to model its propagation characteristics, one should bear in mind the presence of three phenomena in the fiber channel, which are different in nature, occur simultaneously, and influence each other, namely: noise, filtering, and Kerr nonlinearity [3],[4].

This publication is mainly concerned with the filtering phenomenon which stems from the fiber's dispersion. There are two distinct origins to the dispersive nature of fibers: waveguide and material. For instance, a fused silica SSMF operating at 1550nm wavelength exhibits a combined dispersion D which amounts to 16ps/nm.km.

In the modeling the fiber is considered to be linear with constant loss $\alpha\,[\mathrm{dB/km}]$, whereas the phase factor $\beta(\omega)$ exhibits dependence with respect to the frequency deviation according to the Taylor's series as shown

$$\beta(\omega)=\beta(\omega_o)+\beta'(\omega_o)(\omega-\omega_o)+\frac{1}{2}\beta''(\omega_o)(\omega-\omega_o)^2 \qquad (13)$$

It is worthwhile to point out that the three parcels on the right hand side display distinct dependence with respect on the frequency deviation: the first one is constant, the second varies linearly and is related to the group time delay, whereas the third one has a quadratic dependence and is related to the fiber chromatic dispersion (D), optical carrier wavelength (λ_o), and speed of light (c) in vacuum, according to following expression

$$\beta''(\omega_o)=-\frac{D\lambda_o^2}{2\pi c} \qquad (14)$$

At the output end of the SSMF a square law photodetector (PD), transform the photon stream into a RF electric current. Introducing the concept of PD responsivity it can be shown that the electrical photocurrent is proportional to the incident average optical power, hence it is proportional to the magnitude of the optical Poynting vector. Assuming a uniform power distribution over the fiber cross section, the time dependent RF current is given by

$$i(t)=\Re\frac{\left|e_f(t)\right|^2}{2\xi}+n(t)=\Re\frac{E_f(t)E_f^*(t)}{2\xi}+n(t) \qquad (15)$$

where $\Re$ is the PD responsivity and ξ is a constant which depends on both the fiber effective cross section and the optical wave impedance. The $n(t)$ term accounts for additive noises sources such as thermal and shot noises [15]. However, this noise subject will not be addressed in this publication.

As will be shown latter in this publication, (15) reveals that by applying the fiber output to the PD, beating signals between the optical spectral components will generate harmonics of the original RF modulating signal. The characteristics of these signals depend on both the fiber optic chromatic dispersion and the modulation format. Such dependence will be used to estimate the link performance. In practical terms such study may be carried out using an electronic spectrum analyzer (ESA), connected to the PD, as suggested in Fig. 1.

III. Optical Fiber Link Model

As previously stated this publication is concerned with links based on DD-MZM having a 50/50 splitting ratio. Hence using (11), the output electrical field, in the complex form, turns out to be expressed as

$$\begin{aligned} E_{MZM}(t) &= \frac{E_o}{2}e^{j\omega_o t}\left\{e^{j[m_1\cos(\omega_{RF}t+\theta_1)+\theta_2]}+e^{jm_2\cos(\omega_{RF}t)}\right\} \\ &= \frac{E_o}{2}e^{j\omega_o t}\left[\sum_{n=-\infty}^{+\infty} j^n J_n(m_1)e^{jn(\omega_{RF}t+\theta_1)}e^{j\theta_2}+\right. \\ &\qquad \left. +\sum_{n=-\infty}^{+\infty} j^n J_n(m_2)e^{jn\omega_{RF}t}\right] \end{aligned} \qquad (16)$$

where $J_n(\cdot)$ represents the first kind Bessel function with order n.

By rewriting (16) in the following way

$$E_{MZM}(t)=\frac{E_o}{2}e^{j\omega_o t}\sum_{n=-\infty}^{+\infty} a_n e^{jn\omega_{RF}t} \qquad (17)$$

where

$$a_n = j^n\left[J_n(m_1)e^{j(n\theta_1+\theta_2)}+J_n(m_2)\right] \qquad (18)$$

It is readily seen that the optical field at the output of the DD-MZM indeed consist of an infinite series of optical spectral components with frequency $\omega=\omega_o+n\omega_{RF}$ and amplitude a_n, as previously stated. Using (17) and assuming that $m_1=m_2=m<<1$, one obtains an approximated and rather helpful expression for the optical field at the output of the modulator, which is shown below

$$E_{MZM}(t)\approx\frac{E_o}{2}e^{j\omega_o t}\left(a_{-1}e^{-j\omega_{RF}t}+a_0+a_{+1}e^{j\omega_{RF}t}\right) \qquad (19)$$

where

$$a_{\pm1}=|a_{\pm1}|e^{j\phi_{\pm1}} \quad , \quad a_0=|a_0|e^{j\phi_0} \qquad (20.a)$$

$$|a_{\pm1}|=2\left|J_1(m)\cos\left(\frac{\theta_1\pm\theta_2}{2}\right)\right| \quad , \quad |a_0|=2\left|J_0(m)\cos\left(\frac{\theta_2}{2}\right)\right| \qquad (20.b)$$

$$\phi_{\pm1}=\frac{\theta_2\pm\theta_1}{2}+\frac{\pi}{2} \quad , \quad \phi_0=\frac{\theta_2}{2} \qquad (20.c)$$

As an illustration of the usefulness of such approach, we would like to point out that it enables one to identify the requirement which should be satisfied by the DD-MZM drive electronics in order to provide certain modulation formats. For example, single sideband (OSSB), double sideband (ODSB), and carrier suppressed (OCS) optical modulation formats can be obtained when the pair of parameters (θ_1, θ_2) obeys the following constraint $(\pi/2, \pm\pi/2)$, $(\pi, \pm\pi/2)$, and (π, π), respectively [16]-[20].

Now we return to the exact expression (17) in order to further develop the analysis of the link. Taking into account the linear nature of the fiber optic, and bearing in mind the spectral composition of the optical field at the output of the DD-MZM, we tackled the effect of the chromatic dispersion with the help of (13). In this way we obtained the following expression for the phase factor of an optical spectral component with frequency equal to $\omega = \omega_o + n\omega_{RF}$

$$\beta(\omega_o + n\omega_{RF}) = \beta(\omega_o) + \beta'(\omega_o) n\omega_{RF} + \frac{1}{2}\beta''(\omega_o)(n\omega_{RF})^2 \quad (21)$$

Using the above given result in combination with Maxwell's equations we undertook the time domain analysis of the propagation of the optical field given by (17) along a linear SSMF. The obtained expression for the output electrical field after a fiber length L is given by

$$E_f(t) = 10^{\frac{-\alpha_{dB} L}{20}} \frac{E_o}{2} e^{j\omega_o t} \sum_{n=-\infty}^{+\infty} a_n e^{jn\omega_{RF} t} e^{j\frac{1}{2}(n\omega_{RF})^2 \beta''(\omega_o) L} \quad (22)$$

where α [dB/km] is the fiber optic attenuation.

Once more we remember the linear characteristics of the fiber optics under consideration, therefore it might be possible to benefit from standard techniques developed for frequency domain analysis of system. Aiming at such possibility, first we take the Fourier transform of (22) of linear systems. After some mathematical manipulation, we obtained the following expressions for the electrical field and its complex conjugate, in the frequency domain, respectively

$$E_f(\omega) = 10^{\frac{-\alpha_{dB} L}{20}} \pi E_o \sum_{n=-\infty}^{+\infty} a_n \delta(\omega - n\omega_{RF}) e^{j\frac{1}{2}(n\omega_{RF})^2 \beta''(\omega_o) L} \quad (23.a)$$

$$E_f^*(\omega) = 10^{\frac{-\alpha_{dB} L}{20}} \pi E_o \sum_{k=-\infty}^{+\infty} a_k^* \delta(\omega + k\omega_{RF}) e^{-j\frac{1}{2}(k\omega_{RF})^2 \beta''(\omega_o) L} \quad (23.b)$$

where δ represents the Dirac delta function.

As illustrated in Fig. 1, we are considering the utilization of an electronic spectrum analyzer to detect the RF current at the output of the PD. Therefore, we must be able to use the model to predict dependence on frequency of such current. To this aim, we first remember that the convolution theorem can be applied to rewrite the time domain expression of the PD current, as given (15), in the frequency domain, as shown in the next expression

$$I(\omega) = \frac{\Re E_f(\omega) * E_f^*(\omega)}{4\pi\xi} \quad (24)$$

where the mathematical symbol $*$ denote convolution. Before going any further we substituted (12) into (23.a) and (23.b), in order to be able to express the PD current in terms of the laser power P_o. Then we performed the convolution previously indicated and obtained the following expression for the RF current Fourier's transform, under the condition $n = N + k$,

$$I(\omega) = 2\pi \sum_{N=-\infty}^{+\infty} I(N\omega_{RF}) \delta(\omega - N\omega_{RF}) \quad (25)$$

where

$$I(N\omega_{RF}) = 10^{\frac{-\alpha_{dB} L}{10}} \frac{\Re P_o}{4} e^{j\frac{N\phi}{2}} \sum_{k=-\infty}^{+\infty} a_{N+k} a_k^* e^{jk\phi} \quad (26)$$

and

$$\phi = N\omega_{RF}^2 \beta''(\omega_o) L \quad (27)$$

It is worth noting that (25) and (26) were obtained without introducing any approximation and are in perfect agreement with results published by many authors [6],[7]. Until a few years ago, using such formulas to predict the spectral components of the PD current was rather cumbersome and yielded little physical insight, except when one assumed a small signal approximation. It is worth to remember such complexity mostly stems from the fact that the coefficient $a_{N+k} a_k^*$ involves the product of Bessel's function, as it is readily seen in (18). However, a few years ago such drawback was overcome through the application of Graf's addition theorem for Bessel functions [7],[21].

In order to be able to take advantage of such theorem in the analysis presented in this publication, we first use (18) to calculate $a_{N+k} a_k^*$ and then substitute the obtained result into (26). After some mathematical manipulations we obtained an expression for $I(N\omega_{RF})$, which beyond allowing the retrieving of previous results also includes a few parameters such as the fiber attenuation, PD responsivity and laser output power, which were not explicitly accounted for in previous publications. Such expression is given by

$$\begin{aligned} I(N\omega_{RF}) &= 10^{\frac{-\alpha_{dB} L}{10}} \frac{\Re P_o}{4} \times \\ &\times \left\{ e^{jN\left(\theta_1 + \frac{\phi+\pi}{2}\right)} \sum_{k=-\infty}^{+\infty} J_{N+k}(m_1) J_k(m_1) e^{jk\phi} + \right. \\ &+ e^{jN\left(\frac{\phi+\pi}{2}\right)} \sum_{k=-\infty}^{+\infty} J_{N+k}(m_2) J_k(m_2) e^{jk\phi} + \\ &+ e^{j\left[N\left(\theta_1 + \frac{\phi+\pi}{2}\right) + \theta_2\right]} \sum_{k=-\infty}^{+\infty} J_{N+k}(m_1) J_k(m_2) e^{jk(\phi+\theta_1)} + \\ &\left. + e^{j\left[N\left(\frac{\phi+\pi}{2}\right) - \theta_2\right]} \sum_{k=-\infty}^{+\infty} J_{N+k}(m_2) J_k(m_1) e^{jk(\phi-\theta_1)} \right\} \end{aligned} \quad (28)$$

Since we intend to compare our predictions with previous publication, we apply the Graf's addition theorem for Bessel functions [22] to (28) under the assumption that the modulation indexes are equal [6],[7]

$$\begin{aligned} I(N\omega_{RF}) = {} & 10^{\frac{-\alpha_{dB}L}{10}}\frac{\Re P_o}{4}\times \\ & \times\left\{\left[e^{jN(\theta_1+\pi)}+e^{jN\pi}\right]J_N\left[2m\sin\left(\frac{\phi}{2}\right)\right]+\right. \\ & +e^{j\left[N\left(\frac{\theta_1}{2}+\pi\right)+\theta_2\right]}J_N\left[2m\sin\left(\frac{\phi+\theta_1}{2}\right)\right]+ \\ & \left.+e^{j\left[N\left(\frac{\theta_1}{2}+\pi\right)-\theta_2\right]}J_N\left[2m\sin\left(\frac{\phi-\theta_1}{2}\right)\right]\right\} \end{aligned} \tag{29}$$

In this publication, the modeling of the analog fiber optic link is synthesized by (29). It enables the RF frequency domain analysis of how the fiber optic chromatic dispersion affects the performance of links which employ DD-MZM. The optical modulation format can be specified by properly selecting the parameters θ_1 and θ_2. This publication follows the approach adopted in [7], according to which the bias θ_2 can varies within a certain range, by change the bias voltage, whereas the phase θ_1 is restricted to certain values. The two situations addressed in [7], which also are treated in this publication, are obtained when either $\theta_1=\pi$ or $\theta_1=\pi/2$. The corresponding RF current Fourier's transform, obtained using (29), are, respectively

$$\begin{aligned} I(N\omega_{RF},\theta_2)\Big|_{\theta_1=\pi} = {} & 10^{\frac{-\alpha_{dB}L}{10}}\frac{\Re P_o}{4}\times \\ & \times\left\{\left[1+(-1)^N\right]J_N\left[2m\sin\left(\frac{\phi}{2}\right)\right]+\right. \\ & +(-j)^N\cos(\theta_2)\left\{J_N\left[2m\cos\left(\frac{\phi}{2}\right)\right]+\right. \\ & \left.+J_N\left[-2m\cos\left(\frac{\phi}{2}\right)\right]\right\} \\ & +j(-j)^N\sin(\theta_2)\left\{J_N\left[2m\cos\left(\frac{\phi}{2}\right)\right]-\right. \\ & \left.\left.-J_N\left[-2m\cos\left(\frac{\phi}{2}\right)\right]\right\}\right\} \end{aligned} \tag{30.a}$$

$$\begin{aligned} I(N\omega_{RF},\theta_2)\Big|_{\theta_1=\pi/2} = {} & 10^{\frac{-\alpha_{dB}L}{10}}\frac{\Re P_o}{4}e^{\frac{N5\pi}{4}}\times \\ & \times\left\{2\cos\left(\frac{N\pi}{4}\right)J_N\left[2m\sin\left(\frac{\phi}{2}\right)\right]+\right. \\ & +e^{j\theta_2}J_N\left[2m\sin\left(\frac{\phi}{2}+\frac{\pi}{4}\right)\right] \\ & \left.+e^{-j\theta_2}J_N\left[2m\sin\left(\frac{\phi}{2}-\frac{\pi}{4}\right)\right]\right\} \end{aligned} \tag{30.b}$$

Usually the fiber link's performance is evaluated in terms of the RF power spectrum at the output load, i.e. at the input of the ESA, as suggested in Fig. 1. To this aim we recognize that average power of the harmonic with order N which is delivered to the load is given

$$P_{R_L} = \frac{|I(N\omega_{RF})|^2 R_L}{2} \tag{31}$$

where R_L is the load resistance and $I(N\omega_{RF})$ is given by (30.a) and (30.b).

IV. Numerical Results and Discussion

The numerical simulations developed based on (31) were carried out using link components with the characteristics specified in Table I.

TABLE I. TYPICAL VALUES OF PARAMETERS USED IN THE SIMULATION.

Parameter	Symbol	Value
RF source input impedance	Z_g	50Ω
RF load impedance	Z_L	50Ω
RF power applied to DD - MZM	P_{RF}	10mW
Laser optical power	P_o	1mW
Laser wavelength	λ_o	1550nm
DD - MZM half-wave voltage	V_π	5V
DD - MZM input impedance	Z_{MZM}	50Ω
Fiber optic attenuation	α_{dB}	0.2dB/km
Fiber optic chromatic dispersion	D	16ps/nm.km
Speed of light	c	$3\text{x}10^8$m/s
PD responsivity	$\Re$	0.5A/W

Aiming to validate our model, first of all we developed simulation with exactly the same link parameters used in [7]. Part of the results are presented in Fig. 2 and show the dependence of the output RF power for fundamental $(N=1)$ and second harmonic normalized to the detected DC power versus the parameter ϕ. This parameter, which is given in (27), beyond taking into account the chromatic dispersion (D), also depends on both the RF frequency and the fiber length. The simulation was carried out with θ_1 fixed and obeying the constraint set by either ODSB or OSSB whereas θ_2 was allowed to assume any value. Bearing in mind that when $N=1$ and $(\theta_1,\theta_2)=(\pi,\pm\pi/2)$ the DD-MZM yields ODSB modulation, one redly concludes with base in Fig. 2 that fundamental RF power strength is strongly affected by the chromatic dispersion to such an extent that when $\phi/2\pi=0.5$ its power is reduced to zero. This is the so called notch filter like behavior. With respect to the second harmonic, Fig. 2 also shows that upon to the selection of the phase shift θ_2 it can exhibits all-pass, band-pass, and band-stop like behavior with respect to the parameter ϕ.

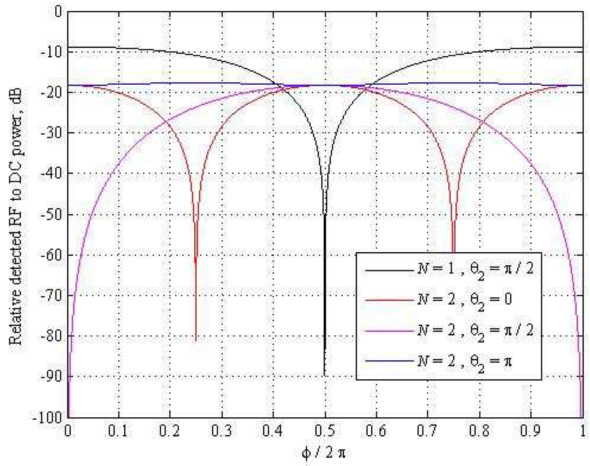

Fig. 2. Detected RF signal power for the fundamental $(N=1)$ and its second harmonic $(N=2)$ normalized to the detected DC level versus $\phi/2\pi$, as predicted by (30.a) with $\theta_1 = \pi$.

Now we turn our attention to the situation in which the requirement $\theta_1 = \pi/2$. The simulation was performed in a fashion very much like the previous case and the results are depicted in Fig. 3. With respect to such illustration, we would like to point out that it reveals that when the drive electronics reaches the condition $(\theta_1, \theta_2) = (\pi/2, \pm\pi/2)$, i.e., when the DD-MZM yields OSSB modulation, the link exhibits the special feature of RF fundamental power displaying very low sensitivity with respect to both the fiber length and the RF frequency. Such unique feature has been widely exploited in practical applications, most of them in the long haul fiber optical telecommunications.

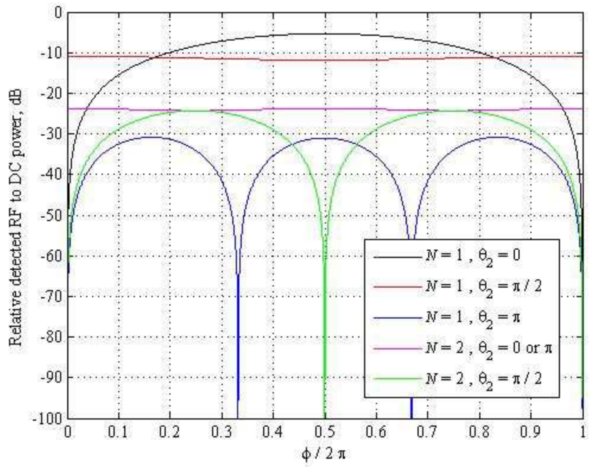

Fig. 3. Detected RF signal power for the fundamental $(N=1)$ and its second harmonic $(N=2)$ normalized to the detected DC level versus $\phi/2\pi$, as predicted by (30.b) with $\theta_1 = \pi/2$.

Still with respect to Fig. 3, it reveals that as the drives electronics departs from the condition $(\theta_1, \theta_2) = (\pi/2, \pm\pi/2)$ even the fundamental RF power can becomes very much frequency dependent. The results presented in Fig. 2 and 3 are in perfect agreement with [7]. In order to be able to better illustrate the effect of the chromatic dispersion in the fundamental and second harmonic RF power it is convenient to analyze its dependence with respect to either the fiber's length or the RF frequency. To this aim we first tackled the ODSB modulation, $(\theta_1, \theta_2) = (\pi, \pm\pi/2)$, and with data from Table I performed a few simulations based on (30.a) and (31). Parts of the results obtained are shown in Fig. 4.

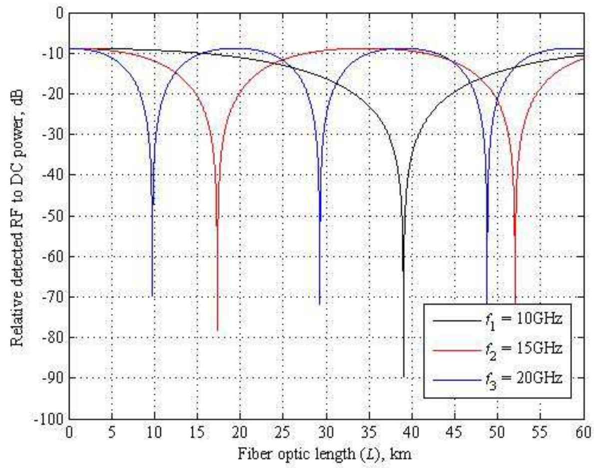

Fig. 4. Detected RF signal power for the fundamental, normalized to the DC level versus fiber length (L) with RF frequency as a parameter.

As can be seen in Fig. 4, irrespective of the RF frequency, the chromatic dispersion results in a periodic variation of the normalized RF power as the fiber length is increased. The position along the fiber at which the RF power is cancelled out depends on the RF frequency. For example, when the RF frequency is 20GHz the first minimum occurs at approximately 10km, whereas for a 10GHz frequency the first minimum is reached at nearly 40km. Such feature has been playing a major role on subject of microwave photonics [1],[2]. The formulation also enables the analysis of ODSB link's sensitivity with respect to drive electronic drift. The fundamental RF power dependence on the deviation from the condition $(\theta_1, \theta_2) = (\pi, \pm\pi/2)$ due to θ_2 is depicted in Fig. 5.

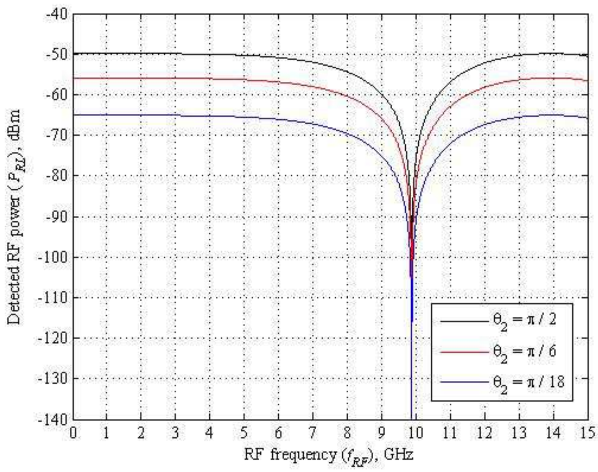

Fig. 5. Fundamental RF output power (P_{RL}) versus the RF frequency (f_{RF}), using (30.a) with θ_2 as a parameter, $\theta_1 = \pi$ and $L = 40\text{km}$.

The results given in Fig. 5 show that irrespective of the bias (θ_2) the RF fundamental power exhibits frequency dependence with a notch like behavior. The particular situation under consideration comprises a SSMF with length equal to 40km which implies a minimum in the RF transmission occurring at nearly 10GHz. However, one should notice that on both sides of the notch frequency the transmission is coefficient is affected by the bias's drift.

We now extend the analysis in order to be able to undertake the study of the dependence of the second harmonic RF power on the RF frequency as the link operates away from the condition $(\theta_1, \theta_2) = (\pi, \pm\pi/2)$. Parts of the simulated results are shown in Fig. 6. For the sake of comparison the figure also shows some of the results obtained for the RF power at the fundamental frequency, which were just discussed. We would like to emphasize that Fig. 6 looks very much similar to Fig. 2, as expected. However, the former may be very helpful, especially for the experimentally oriented researcher, because it uses as coordinate axes measurable quantities.

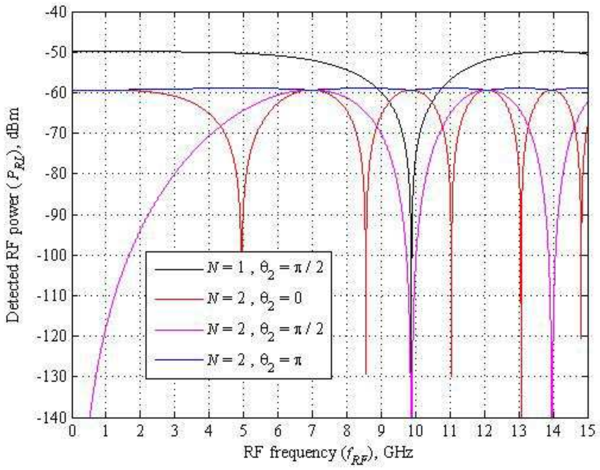

Fig. 6. Fundamental RF output power $(N = 1)$ and its second harmonic $(N = 2)$ versus the RF frequency (f_{RF}), based on (30.a) with $L = 40\text{km}$.

We now turn our attention to the links which are modeled with base in (30.b). As already pointed out in this publication in such type the DD-MZM yields OSSB modulation provided by the condition $(\theta_1, \theta_2) = (\pi/2, \pm\pi/2)$ is satisfied. Moreover, results of the obtained using the formulation here presented in the modeling of its performance, which are partially given in Fig. 3, show perfect agreement with previous publication [7]. For practical reason and the sake of uniformity it is worthwhile to redraw the graphics shown in Fig. 3 using coordinate axes identical to those used in Fig. 6. The parameters given in Table I were employed in (30.b) and the obtained result for the RF fundamental power at the output of a link with $L = 40\text{km}$ are shown in Fig. 7. It readily seen that when the drive electronics yields an OSSB modulation the RF fundamental power level is nearly flat as the RF frequency sweeps.

However, as the DD-MZM bias drifts away from the optimum value $(\theta_2 = \pi/2)$ the RF fundamental power becomes so strongly dependent on the RF frequency that even notch filter like behavior are observed. However, it is important to observe that some power level advantage may be profited while operating away from the exact OSSB requirement, as it is shown in Fig. 7 when $\theta_2 = 0$ and the RF frequency varies within the 6GHz to 13GHz range.

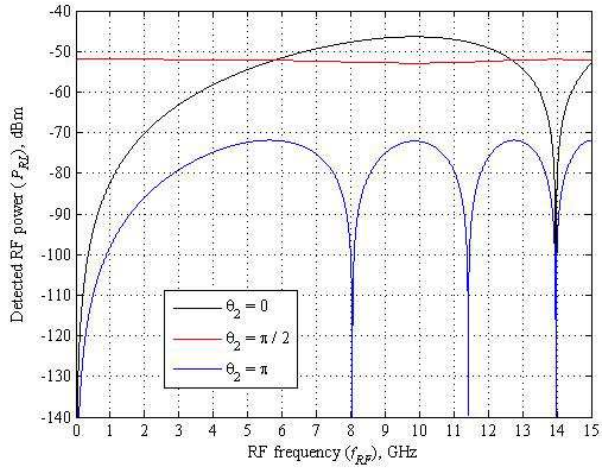

Fig. 7. Fundamental RF output power (P_{RL}) versus the RF frequency (f_{RF}), using (30.b) with θ_2 as a parameter, $\theta_1 = \pi/2$ and $L = 40\text{km}$.

Next we apply to the OSSB case a procedure similar to the one adopted while studying the fundamental and second harmonic RF output power of an ODSB link with respect to the RF frequency, however using (30.b) rather than (30.a). The obtained results for a link with length equal to 40km are shown in Fig. 8. It is worth to point out that this also contains the data on the RF power at the fundamental, which were already shown in Fig. 7.

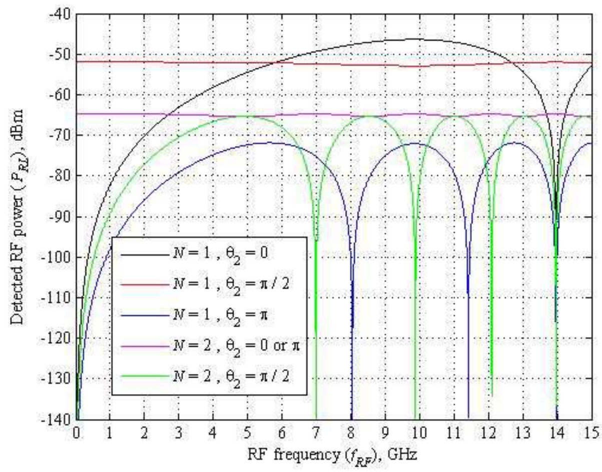

Fig. 8. Fundamental RF output power $(N = 1)$ and its second harmonic $(N = 2)$ versus the RF frequency (f_{RF}), based on (30.b) with $L = 40\text{km}$.

The numerical simulation also enabled the identification of a few link configurations which displays rather interesting characteristics, which are partially summarized in Fig. 9. For instance, it is worthwhile to notice that the RF second-order harmonic power level exhibit a flat dependence with respect to the RF frequency throughout a very wide range. Such feature may be of practical interest in the area of photonic microwave generation.

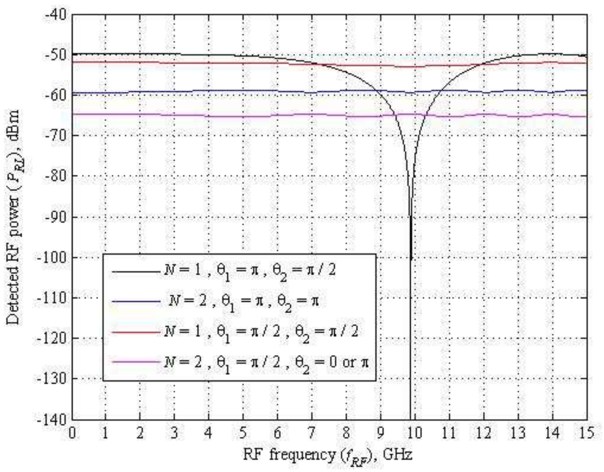

Fig. 9. Detected RF output power for fundamental $(N = 1)$ and its second-order harmonic $(N = 2)$ versus the RF frequency (f_{RF}), with $L = 40\text{km}$.

V. Conclusion

This publication presented a very comprehensive analytical model which enables the analysis of the effect of fiber optic chromatic dispersion in the performance of analog fiber optic link with DD-MZM modulator. The model besides relaying on variables which are suited to experimentally guided researchers, also allows one to retrieve import results available in a very wide literature. Using some state of the art components and devices we performed numerical simulations which yielded results which seem to be of practical interest. The authors are working towards designing, implementing and characterizing fiber link based on the model developed.

Acknowledgments

The authors would like to thank the Electronic Warfare Laboratory at Technological Institute of Aeronautics (ITA) and the National Institute of Telecommunications (INATEL) for their support in this research.

References

[1] J. P. Yao, "A tutorial on microwave photonics - Part I," *IEEE Photonics Society Newsletter*, vol. 26, no. 2, pp. 4-12, April 2012.

[2] J. P. Yao, "A tutorial on microwave photonics - Part II," *IEEE Photonics Society Newsletter*, vol. 26, no. 3, pp. 5-12, June 2012.

[3] R. J. Essiambre, G. Kramer, P. J. Winzer, G. J. Foschini, B. Goebel, “Capacity Limits of Optical Fiber Networks,” *Journal of Lightwave Technology*, vol. 28, no. 4, pp.662-701, February 2010.

[4] J. Wang, K. Petermann, “Small Signal Analysis for Dispersive Optical Fiber Communication Systems,” *Journal of Lightwave Technology*, vol. 10, no. 1, pp. 96-100, January 1992.

[5] A. Yariv, P. Yeh, *Photonics: Optical Electronics in Modern Communications*, 6th ed., New York: Oxford University Press, 2007.

[6] J. L. Corral, J. Marti, and J. M. Fuster, “General expressions for IM/DD dispersive analog optical links with external modulation or optical up-conversion in Mach–Zehnder electrooptical modulator,” *IEEE Transactions on Microwave Theory and Techniques.*, vol. 49, no. 10, pp. 1968–1976, October 2001.

[7] L. Cheng, S. Aditya, A. Nirmalathas, “An Exact Analytical Model for Dispersive Transmission in Microwave Fiber-Optic Links Using Mach-Zehnder External Modulator,” *IEEE Photonics Technology Letters*, vol. 17, no. 7, pp. 1525-1527, July 2005.

[8] C. Lin, J. Chen, S. Dai, P. Peng, S. Chi, “Impact of Nonlinear Transfer Function and Imperfect Ratio of MZM on Optical Up-Conversion Employing Double Sideband With Carrier Suppression Modulation,” *Journal of Lightwave Technology*, vol. 26, no. 15, pp. 2449-2459, August 2008.

[9] Y. Shi, L. Yan, A. E. Willner, “High-Speed Electrooptic Modulator Characterization Using Optical Spectrum Analysis,” *Journal of Lightwave Technology*, vol. 21, no. 10, pp. 2358-2367, October 2003.

[10] X. Chen, S. Feng, D. Huang, “Impact of Mach-Zehnder Modulator Chirp on Radio over Fiber Links,” *Journal of Infrared, Millimeter and Terahertz Waves*, vol. 30, no. 7, pp. 770–779, 2009.

[11] C. E. Rogers III, J. L. Carini, J. A. Pechkis, P. L. Gould, “Characterization and compensation of the residual chirp in a Mach-Zehnder-type electro-optical intensity modulator,” *Optics Express*, vol. 18, no. 2, pp. 1166-1176, January 2010.

[12] C. Kitano, J. E. B. Oliveira, “Projeto de Moduladores Eletroópticos Faixa Larga Utilizando Tecnologia de Óptica Integrada,” *Revista Telecomunicações*, vol. 2, no. 2, pp. 5-16, setembro 1999.

[13] C. Kitano, J. E. B. Oliveira, “Dispositivos à Óptica Integrada para Aplicações em Telecomunicações,” *Revista Telecomunicações*, vol. 3, no. 2, pp. 27-38, dezembro 2000.

[14] J. E. B. Oliveira, J. A. J. Ribeiro, “Interfaces para Enlaces de Fibra Óptica de Alta Velocidade,” *Revista Telecomunicações*, vol. 3, no. 2, pp.65-75, dezembro 2000.

[15] W. Lim, T. S. Cho, K. Kim, C. Yun, “Analytical time-domain model for radio over free space optical military communication systems under turbulence channels,” in *IEEE Military Communications Conference MILCOM 2009*, Paper 901734, pp. 1-5, October 2009.

[16] W. S. Fegadolli, J. E. B. Oliveira, V. R. Almeida, “Highly linear electro-optic modulator based on ring resonator,” *Microwave and Optical Technology. Letters*. vol. 53, no. 10, pp. 2375-2378, October 2011.

[17] M. Morant, R. Llorente, J. Hauden, T. Quinlan, A. Mottet, S. Walker, “Dual-drive $LiNbO_3$ interferometric Mach-Zehnder architecture with extended linear regime for high peak-to-average OFDM-based communication systems,” *Optics Express*, vol. 19, no. 26, pp. 450-456, December 2011.

[18] B. Vidal, "Analytical model for hybrid amplitude and phase modulation in dispersive radio over fiber links," *Optics Communications*, vol. 284, no. 21, pp. 5138–5143, October 2011.

[19] O. L. Coutinho, V. R. Almeida, C. S. Martins, J. E. B. Oliveira, “Aplicação de Enlace a Fibra Óptica em Transmissão de Sinais de Radar,” *Simpósio Brasileiro de Microondas e Optoeletrônica - MOMAG*, Florianópolis, SC, setembro 2008.

[20] G. H. Smith, D. Novak, Z. Ahmed, “Technique for optical SSB generation to overcome dispersion penalties in fibre-radio systems,” *Electronics Letters*, vol. 33, no. 1, pp. 74-75, January 1997.

[21] H. Chi, J. Yao, “Power Distribution of Phase-Modulated Microwave Signals in a Dispersive Fiber-Optic Link,” *IEEE Photonics Technology Letters*, vol. 20, no. 4, pp. 315-317, February 2008.

[22] M. Abramowitz, I. Stegun, *Handbook of Mathematical Functions with Formulas, Graphs, and Mathematical Tables*, New York: Dover Publications, 1965.